THE JOURNAL OF PHYSICAL CHEMISTRY Letters

pubs.acs.org/JPCL

Letter

Yttrium–Sodium Halides as Promising Solid-State Electrolytes with High Ionic Conductivity and Stability for Na-Ion Batteries

Yu Qie, Shuo Wang, Sijie Fu, Huanhuan Xie, Qiang Sun,* and Puru Jena

Cite This: *J. Phys. Chem. Lett.* 2020, 11, 3376–3383

Read Online

ACCESS | Metrics & More | Article Recommendations | Supporting Information

ABSTRACT: All-solid-state sodium-ion batteries (ASIBs) are promising candidates for large-scale energy storage applications. To build such a battery system, efficient solid-state electrolytes (SSEs) with high sodium ionic conductivity at room temperature and good electrochemical stability as well as interface compatibility are required. In this work, using density functional theory combined with molecular dynamics simulation and a phase diagram, we have studied the potential of yttrium halide-based materials (Na_3YX_6, where X = Cl or Br) with inherent cation vacancies as diffusion carriers for solid electrolytes in ASIBs. A great balance between electrochemical stability and ionic conductivity found in these two systems overcomes the shortcomings of sulfide- and oxide-based SSEs. In particular, these two materials show Na^+ conductivities of 0.77 and 0.44 mS cm^{-1} at 300 K and wide electrochemical windows of 0.51–3.75 and 0.57–3.36 V, and good interfacial stability with Na metal anode and high-potential polyanion (fluoro)phosphate cathode materials, respectively. These features make halide-based materials promising efficient solid-state electrolytes for Na-ion batteries.

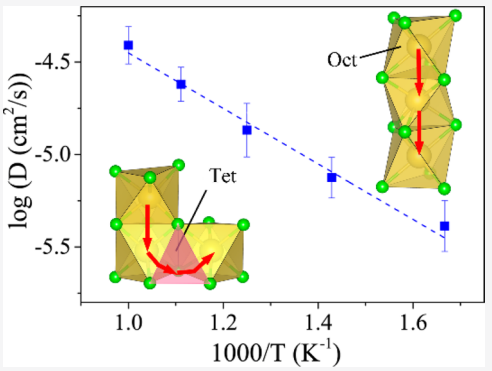

Sodium-ion batteries (SIBs) are considered as a promising alternative to lithium-ion batteries (LIBs) for large-scale energy storage systems because sodium is highly abundant, environmentally friendly, and inexpensive.[1−4] Remarkable progress has been made in developing room-temperature SIBs based on organic liquid electrolytes.[5−7] However, these SIBs suffer from safety issues arising from the volatile and flammable organic liquid electrolytes like their lithium counterparts.[8,9] In this regard, using inorganic nonflammable solid-state electrolytes (SSEs) to prepare all-solid-state sodium-ion batteries (ASIBs) is a good strategy for eliminating the safety concerns caused by liquid electrolytes. In addition, the wide electrochemical window and excellent mechanical properties of SSEs enable the use of high-energy density electrodes such as Na metal anodes and high-voltage cathodes, including Na_2FePO_4F and $Na_3V_2(PO_4)_3$, which further improves the battery performance. This has led to considerable interest in the research on sodium SSEs.[10−14]

For solid-state SIBs, currently most used SSEs are oxides, sulfides, and their derivatives, which face considerable challenges because of an undesirable trade-off between ionic conductivity and stability.[15−17] For example, the oxide solid electrolytes (β-alumina, NASICON, etc.) generally possess good chemical stability and wide electrochemical windows, but most of them exhibit only reasonable ionic conductivities at high temperatures ($\sim 10^{-4}$ S cm^{-1} at room temperature)[18−20] and require harsh synthesis processes for preparing the electrode–oxide SSE composites. This might induce grain-boundary resistance and poor interface contact.[21] In contrast, sulfide-based materials (Na_3PS_4 and other derivatives) are known for their higher ionic conductivities and easier synthetic method of simple cold pressing but suffer from an intrinsic narrow electrochemical stability window and serious interface side reaction.[22−24] To facilitate pragmatic large-scale ASIB applications, developing sodium SSEs with high RT ionic conductivity and a wide electrochemical stability window at the same time is imperative.

Recently, a new class of lithium halide materials have been reported as attractive SSEs for LIBs with high RT ionic conductivities, excellent interface compatibility, and wide electrochemical windows.[25] Wang et al. further confirmed that the smooth energy landscape is intrinsic in a halogen anion sublattice, and the high anodic stability originates from the antioxidant halogen anions.[26] Moreover, Sun et al. successfully synthesized a Li_3InCl_6 SSE and experimentally proved its superior Li-ion conductivity, excellent electrochemical stability, and high stability in ambient air.[27,28] Considering the similarity between LIBs and SIBs, the question of whether halide-based materials can be used as

Received: January 2, 2020
Accepted: April 13, 2020
Published: April 13, 2020

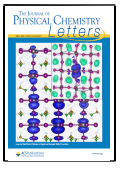

https://dx.doi.org/10.1021/acs.jpclett.0c00010
J. Phys. Chem. Lett. 2020, 11, 3376–3383

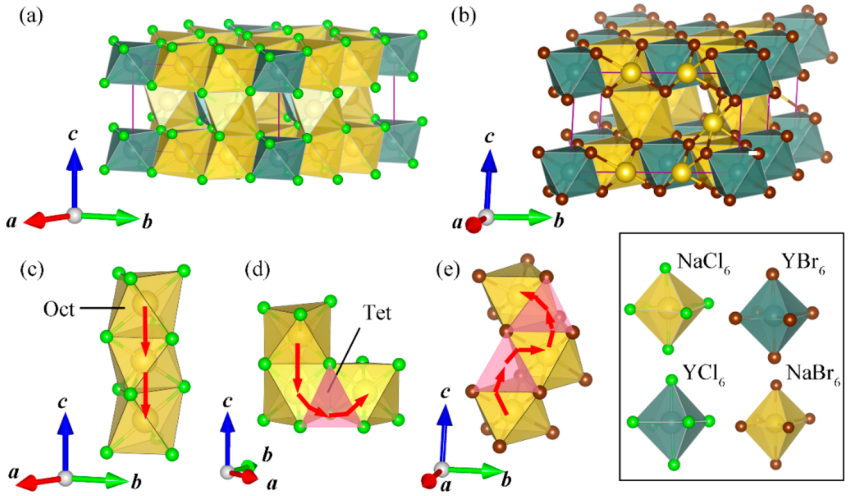

Figure 1. Crystal structures of (a) NYC and (b) NYB. (c) Face-to-face and (d) edge-to-edge connected $NaCl_6$ octahedra in NYC. (e) Edge-to-edge connected $NaBr_6$ octahedra in NYB. The octahedra and tetrahedra are shown as yellow and pink polyhedra, respectively. Na, Y, Cl, and Br atoms are represented as yellow, teal, green, and brown spheres, respectively.

SSEs for SIBs with both high ionic conductivity and good stability naturally arises.

To address this question, in this study, we investigate the ionic diffusivity, electrochemical window, and interfacial stability of sodium−yttrium halides Na_3YX_6 (X = Cl or Br) using first-principles theory. Our results show that Na_3YCl_6 and Na_3YBr_6 possess high RT Na ionic conductivities of 0.77 and 0.44 mS cm^{-1}, respectively, wide electrochemical windows (around 0.6−3.5 V), and high chemical stability toward traditional NIBs cathodes, especially for the high-potential polyanion cathode materials [for example, Na_2MnPO_4F, $Na_3V_2(PO_4)_3$, etc.]. Moreover, the small reaction energy (<50 meV/atom) between Na metal and NYC (NYB) makes it possible to use the Na metal anode, leading to high-energy density ASIBs. In addition, Na_3YCl_6 and Na_3BrCl_6 are both electronic insulators and possess good phase, thermal, and dynamical stability. All of these features make halide materials promising candidates for sodium SSEs.

COMPUTATIONAL METHODS

Density Functional Theory. In this work, all calculations are based on the density functional theory (DFT) and the Vienna *ab initio* Simulation Package (VASP)[29] within the projector augmented-wave (PAW) approach.[30] Generalized gradient approximation (GGA) with the Perdew−Burke−Ernzerhof (PBE) function[31] is used to account for exchange and correlation potential. The Heyd−Scuseria−Ernzerhof (HSE06) hybrid functional[32,33] is used for an accurate band gap. The parameters in the calculations, including the energy cutoff and k-point density, are consistent with those of Materials Project[34] (MP).

Diffusion and Conductivity. The mean square displacement (MSD) method with elevated temperatures is employed to calculate the diffusivity and conductivity based on *ab initio* molecular dynamics (AIMD) simulations. The data analysis is carried out with the *aimd* module developed under the *pymatgen* python framework.[35−38] More details are provided in the Supporting Information.

Electrochemical Stability. To evaluate the electrochemical stability of NYC and NYB, the grand potential phase diagram of a given phase $[C_{eq}(C, \mu_{Na})]$ with the composition C (C = NYC or NYC) in equilibrium with the chemical potential of element Na is constructed.[39,40] The decomposition reaction energy is defined as

$$\Delta E_D^{open}(\text{phase}, \mu_{Na}) = E_{eq}[C_{eq}(C, \mu_{Na})] - E(\text{phase}) - \Delta n_{Na}\mu_{Na}$$

where μ_{Na} is the chemical potential of Na metal and Δn_{Na} is the number difference of element Na from the original composition C. The given phase is stable within a certain range of μ_{Na} where Δn_{Na} is zero.

Chemical Stability of Interfaces. The interface pseudobinary reaction energy is calculated as

$$\Delta E_D(\text{SE}, \text{electrode}, x) = E_{eq}[C_{interface}(C_{SSE}, C_{electrode}, x)] - E_{interface}(\text{SSE}, \text{electrode}, x)$$

where C_{SSE} and $C_{electrode}$ are the compositions of SSE and electrode materials, respectively, normalized to one atom per formula. x is the molar fraction of the SSE.[41,42] The crystal structure and energy of most materials are obtained from the MP database.[34]

Geometries and Stabilities. As the crystalline structures of Na_3YX_6 (X = Cl or Br) have Na partial occupancies, we first generated all symmetrically distinctive structures (see Figure S1) and then conducted DFT calculations to identify the geometries with the lowest energy for each halide. The ground-state structures are displayed in Figure 1. The optimized Na_3YCl_6 (NYC) structure has a D_3^2 space symmetry group (No. 150, $P321$) consisting of two parallel sets of YCl_6 octahedra arranged along different orientations, which is very different from the structure proposed by Stenzel and Meyer[43] reported in 1993 for Na_3YCl_6 with an $R\bar{3}$ space group (No. 148). Here, the YCl_6 octahedra align in the same direction. Na_3YBr_6 (NYB) possesses an fcc-like anion arrangement with a space symmetry group of C_2^3 (No. 5, $C2$). In both cases, the yttrium and sodium atoms are 6-fold coordinated with halogens, forming NaX_6 and YX_6 (X = Cl or Br) octahedra with high stability.[43] In addition, there are two empty cation sites near the Y site, acting as built-in cation vacancy sites, which play an important role in ion conductivity as known in many SSEs such as Li_xScCl_{3+x},[44] LATP,[45] LGPS,[46] and

https://dx.doi.org/10.1021/acs.jpclett.0c00010
J. Phys. Chem. Lett. 2020, 11, 3376−3383

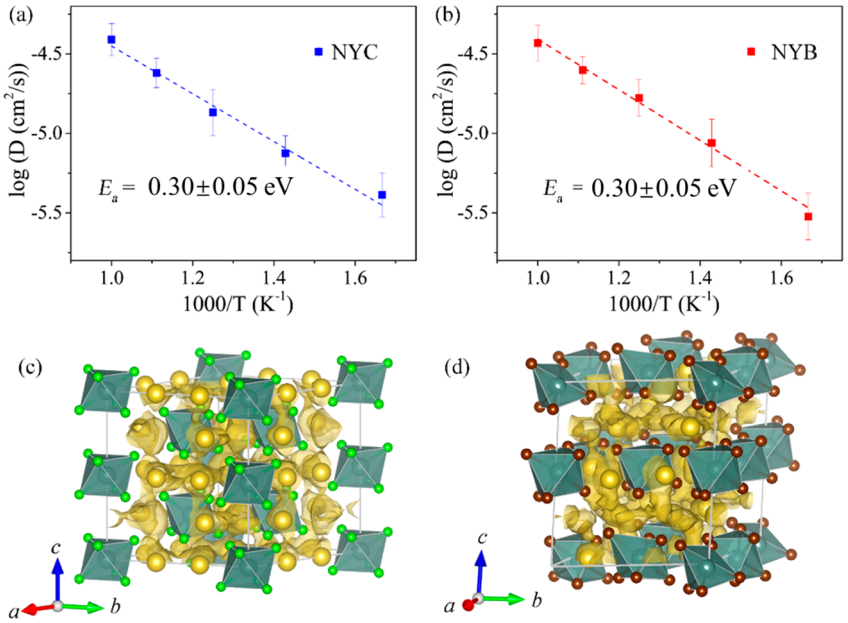

Figure 2. Arrhenius plots of the Na^+ diffusion coefficient in (a) NYC and (b) NYB obtained from AIMD simulations. (c) Isosurface of the Na^+ probability density distribution (yellow) in (c) NYC and (d) NYB at 600 K, with an isosurface value of 0.00025 e/Bohr.[3]

LLZO.[47,48] Such partial occupation sites lead to a smoother energy landscape and act as available sites for ion migration. As presented in Figure 1c, the $NaCl_6$ octahedra are connected in a face-to-face manner along the *c* direction in NYC, where Na ions could migrate along the *c* direction by directly hopping to the adjacent octahedral (Oct) sites, leading to one-dimensional (1D) Na conduction channels. On the other hand, along the *a* and *b* directions, the $NaCl_6$ octahedra are connected in an edge-to-edge manner, making the Na cations migrate via tetrahedral (Tet) sites when hopping to the other Oct sites (Figure 1d). Due to the repulsion from the adjacent Y ion, partial Tet sites are blocked, thus resulting in sluggish Na diffusion along these two directions. For NYB, as one can see from Figure 1b, the $NaBr_6$ octahedra are connected in an edge-to-edge manner in all axis directions. Therefore, the Na ions diffuse in the NYB framework with an Oct-Tet-Oct path (see Figure 1e), where a three-dimensional (3D) isotropic diffusion network can be expected.

Before studying ionic conductivity, we need to check the stability from different perspectives. According to the ternary phase diagrams constructed using DFT results at 0 K (see Figure S2), the ΔE_{above_hull} value of NYC is 8.6 meV per atom, which can be compensated by thermal energy fluctuation at room temperature, and the NYB is exactly on the hull, indicating the thermodynamic stability at 0 K. As shown in panels a and b of Figure S3, after the materials are heated to 300 K for 10 ps, the total energy only fluctuates around a constant value, and the frameworks of NYB and NYC remain nearly intact without apparent distortion. This suggests that NYC and NYB are thermally stable at room temperature. Finally, the phonon spectra are analyzed to examine the dynamical stability, and the results are displayed in panels c and d of Figure S3, where no soft phonon mode exists over the entire Brillouin zone for both NYC and NYB, thus confirming their dynamic stabilities.

Na-Ion Diffusivity and Conductivity. We next discuss the Na-ion migration properties in NYC and NYB, which is one of the key factors for assessing the performance of SSEs. To study Na^+ migration in the yttrium halide-based SSEs, the Arrhenius diagrams of Na^+ diffusivity in NYC and NYB at different temperatures from 600 to 1000 K are plotted in panels a and b of Figure 2, respectively. The activation energies (E_a) of NYC and NYB are derived to be 0.30 ± 0.05 and 0.32 ± 0.05 eV, respectively. Moreover, the extrapolated theoretical diffusivities (D) at 300 K are found to be 1.11×10^{-8} cm^2/s with error bounds of $[1.78 \times 10^{-9}, 6.91 \times 10^{-8}]$ cm^2/s in NYC and 0.76×10^{-8} cm^2/s with error bounds of $[1.02 \times 10^{-9}, 5.57 \times 10^{-8}]$ cm^2/s in NYB. Additionally, as listed in Table 1, the corresponding Na^+ conductivity (σ) at RT for NYC is 0.77 mS/cm with error bounds of [0.12, 4.81] mS/cm, which is comparable to the value of 0.74 mS/cm for Na_3PS_4–Na_4SiS_4[24] and higher than those of c-Na_3PS_4 (0.2 mS/cm),[22] $Na_{10}SnP_2S_{12}$ (0.4 mS/cm),[23] and NASICON-based hybrid SSE (0.36 mS/cm).[49] In particular, it is much higher than the value of 10^{-3} mS/cm reported by Stenzel et al.[43] for Na_3YCl_6 due to the different structure,[50] suggesting that the geometry can significantly change the ion conductivity in a chloride-based solid electrolyte. NYB also possesses a high RT conductivity of 0.44 mS/cm with error bounds of [0.06, 3.22] mS/cm, which is comparable to that of $Na_{10}SnP_2S_{12}$.[23]

Table 1. Comparison of Na^+ Conductivities (σ) at 300 K for NYC–NYB with Other Sodium Solid-State Electrolytes

composition	σ at 300 K (mS/cm)
NYC	0.77
NYB	0.44
c-Na_3PS_4[22]	0.2
$Na_{10}SnP_2S_{12}$[23]	0.4
Na_3PS_4–Na_4SiS_4[24]	0.74
NASICON-based hybrid SSE[49]	0.36
pristine t-Na_3PS_4[51]	0.01
Na_3YCl_6-I[43]	10^{-3} at 500 K (exp)

As shown in Figure 2c for the probability density distribution (PDF), 1D Na-ion diffusion channels indeed

https://dx.doi.org/10.1021/acs.jpclett.0c00010
J. Phys. Chem. Lett. 2020, 11, 3376−3383

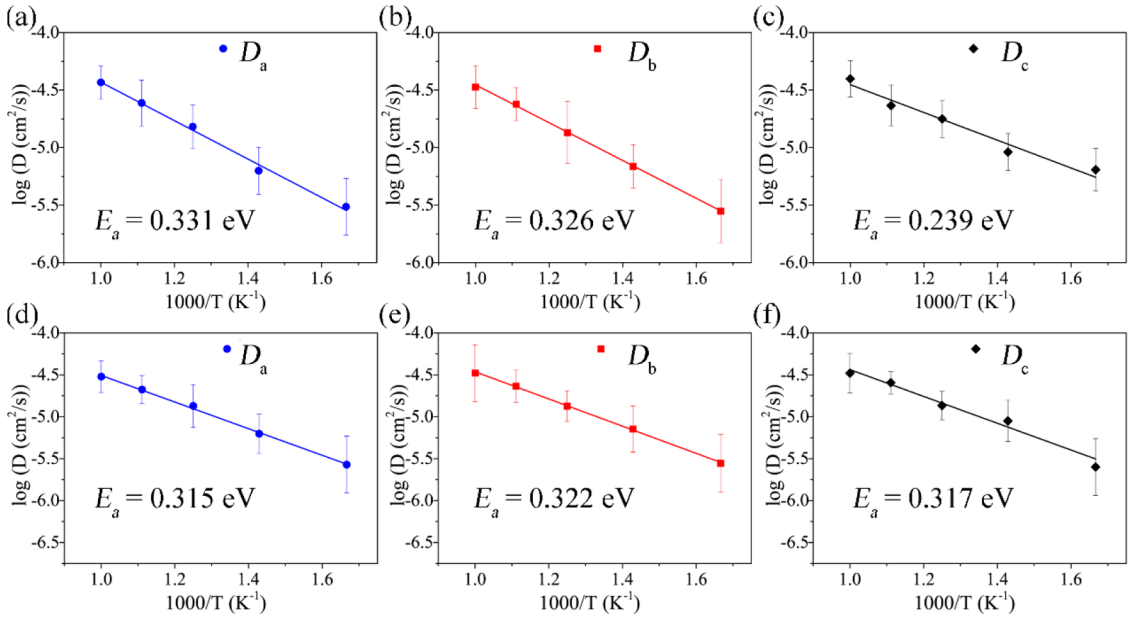

Figure 3. Arrhenius plots of Na^+ diffusion along the *a*, *b*, and *c* directions in NYC (top row) and NYB (bottom row) obtained from AIMD simulations. The activation energies are noted in the diagrams.

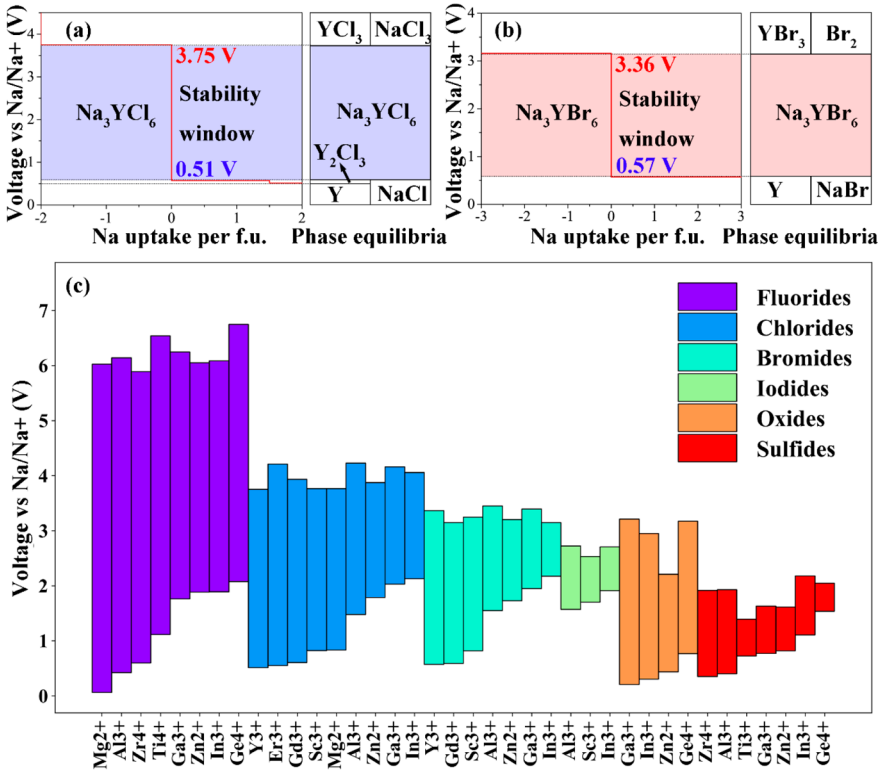

Figure 4. Equilibrium voltage profiles and phase equilibria for sodiation and desodiation reactions of (a) NYC and (b) NYB. (c) Calculated electrochemical windows of Na−M−X ternary compounds, including fluorides, chlorides, bromides, iodides, oxides, and sulfides. M is a metal cation with the highest common valence state.

exist along the *c* direction in NYC. Moreover, from the MSD of Na ions along different directions (see Figure S5a), we find that the MSD values along the *a* and *b* directions are the same in NYC, which is approximately half of that along the *c* direction, suggesting the preference of Na-ion diffusion along the *c* direction. This is consistent with the crystal symmetry and the 1D channel structure of NYC. In contrast, Na ions in NYB diffuse through a 3D isotropic network as suggested by the PDF (Figure 2d) and MSD plot (Figure S5b). On the basis of the values of diffusion coefficient *D* along different directions, the E_a along the *a*, *b*, and *c* directions are calculated via linear Arrhenius fittting, and the results are displayed in Figure 3 and Table S3. In NYC, the corresponding E_a values along the *a* and *b* directions are both 0.33 eV, while the value along the *c* direction is much smaller (0.24 eV), indicating the preferred migration path for Na ions. In the case of NYB, all of

https://dx.doi.org/10.1021/acs.jpclett.0c00010
J. Phys. Chem. Lett. 2020, 11, 3376−3383

the activation energies along the *a*, *b*, and *c* directions have similar values around 0.32 eV, showing an isotropic diffusion behavior.

The different Na-ion diffusion features stem from the different geometrical structures of NYC and NYB. As shown in Figure 1, for NYC, the Na ions migrate along the *c* direction by one-step hopping to the adjacent Oct sites, forming 1D channels. These 1D channels connect with each other in the *a*−*b* plane via Tet interstitial sites, developing a 3D diffusion network. Therefore, the Na^+ diffusion is anisotropic with fast 1D diffusion along the *c* direction. For NYB, the diffusion is isotropic where all of the Na^+ ions hop to the other Oct sites through Tet interstitial sites, leading to a 3D isotropic diffusion network as shown in Figures 2 and 3.

Electrochemical Stability. Apart from the high Na-ion conductivity, an effective SSE candidate should also exhibit good electrochemical stability as well as poor electronic conductivity, which have an influence on the overall performance of ASIBs. As shown in panels a and b of Figure 4, both NYC and NYB hold wide electrochemical windows of [0.51, 3.75] V and [0.57, 3.36] V from the oxidation limits to the reduction limits, respectively. These values are impressive when compared with those of some reported oxide-based and sulfide-based SSEs, including $Na_3Zr_2Si_2PO_{12}$ (1.1−3.4 V), Cl-doped t-Na_3PS_4 (1.2−2.4 V), Na_3AsS_4 (1.9−2.1 V), etc. (Figure S10).[16,52] In spite of the fact that NYC and NYB are thermodynamically unstable with the Na metal electrode at 0 V, the corresponding reactions have extremely small reaction energies (50 and 17 meV/atom for NYC and NYB, respectively) and can even be considered as reversible reactions during thermal fluctuation, indicating the feasibility of using the Na metal anode, which possesses the highest energy density in the ASIB cells. With respect to the oxidation limits, a value of ∼3.5 V allows NYC and NYB to assemble with the high-voltage sodium cathode materials, including a layered metal oxide (such as $NaCrO_2$)[53] and polyanion materials (such as Na_2FePO_4F, $Na_3V_2(PO_4)_3$, etc.).[54−58] This aspect is vital for high-voltage and high-energy density batteries. To deeply analyze the high oxidation stability of NYC and NYB, the electrochemical windows of Na−M−X ternary compounds with different anions (M = cation, and X = F, Cl, Br, I, O, or S) are calculated, and the results are shown in Figure 4c. We can see that almost all halides possess a considerable oxidation voltage of >3 V (except for iodides), superior to those of sulfides and oxides, which illustrates the intrinsic oxidation stability of the halide compounds as the lithium halide SSEs counterparts.[26] In addition, the poor electrical conductivity is necessary for SSEs to avoid further redox reaction inside SSEs.[59] As displayed in DOS (Figure S11), NYC and NYB are insulators with large band gaps of 6.01 and 5.54 eV, respectively, preventing the redox reaction from interface into the bulk inside. The wide electrochemical windows and large band gaps make NYC and NYB promising SSEs for substituting for sulfides and oxide-based materials.

Chemical Interface Stability with Cathode Materials. The interfacial stability between SSEs and cathodes is another crucial aspect of solid-state battery devices. In general, the cathode materials with relatively low average voltages, such as Mo_6S_8 (∼1.4 V vs Na/Na^+)[14] and TiS_2 (∼1.7 V vs Na/Na^+),[16] are used in the assembled ASIBs to match the narrow electrochemical stability window of sulfide-based SSEs. However, the wide μ_{Na} stability windows of NYC and NYB support their usage with high-potential cathode materials, contributing to high-density ASIBs. For a more comprehensive evaluation of the performance of NYC and NYB, we have also investigated the interface chemical stability between NYC (NYB) and currently used cathodes with high potential.[15,17,58] The results are presented in Figure 5, Figure S12, Table 2, and Table S4.

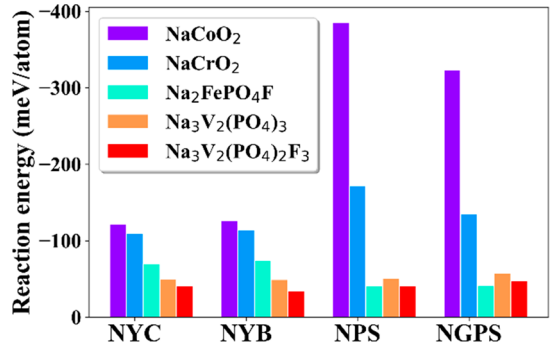

Figure 5. Calculated mutual reaction energies of the SE−cathode interface for (a) NYC, (b) NYB, (c) cubic Na_3PS_4 (NPS), and (d) $Na_{10}GeP_2S_{12}$ (NGPS). Data for the different cathode materials are shown as solid bars with different colors.

The interface mutual reaction energy ($\Delta E_{D,min,mutual}$) diagram is presented in Figure 5; when compared with sulfide electrolyte materials [cubic Na_3PS_4 (NPS) and $Na_{10}GeP_2S_{12}$ (NGPS)], NYC and NYB possess smaller reaction energies with layer cathode materials $NaCoO_2$ and $NaCrO_2$, indicating better stabilities with these two cathodes. To deeply understand the interface reaction, the interface thermodynamic equilibria are also calculated (Table 2 and Table S4). The reaction between NYC and $NaCoO_2$ corresponds to a change from Co^{3+} to Co^{2+} and leads to electrically insulating products, including NaCl, Y_2O_3, $NaClO_4$, and Co_3O_4, while the Co_9S_8 generated at NPS, NGPS, and $NaCoO_2$ interfaces is electronically conductive, which is unfavorable to the stability of the interface.[42,60] In contrast to the NYC−$NaCoO_2$ interface, the reaction at the NYC−$NaCrO_2$ interface would generate a passive coating composed of electron-insulating $YCrO_3$, NaCl, and Cr_2O_3. In addition, it should be noted that at the NYB−$NaCoO_2$ interface, molecular bromine will be generated due to the relatively low oxidation stability of Br anions, which is detrimental for ASIBs. Therefore, the usage of $NaCoO_2$ is limited when NYB is applied as the SSE in cells. In addition, the interfaces between SSEs and polyanion cathodes [Na_2FePO_4F (NFPF), $Na_3V_2(PO_4)_2F_3$ (NVPF), and $Na_3V_2(PO_4)_3$ (NVP)] are explored, as well. With much smaller reaction energies (∼50 meV/atom), the four SSEs are more stable with polyanion cathodes, which can be attributed to the electron-withdrawing character of the PO_4^{3-} group and F^-.[61] The reaction products at the NYC/NYB and NFPF/NVPF/NVP interfaces are sodium salts and phosphates with poor electron conductivity. Note that the lowest value of $\Delta E_{D,min,mutual}$ appeared for the NYB−NVPF interface reaction (35 meV/atom), which can inhibit severe interfacial decomposition, decrease the interfacial resistance, and remain stable performance during cycling, indicating good interface compatibility with high-potential cathodes. Therefore, NYC and NYB compounds are promising SSEs possessing good interfacial compatibility with high-potential cathodes.

In summary, motivated by the recent experimental synthesis of yttrium halides for Li-ion batteries, we carried out systematic

https://dx.doi.org/10.1021/acs.jpclett.0c00010
J. Phys. Chem. Lett. 2020, 11, 3376−3383

Table 2. Phase Equilibria and Minimum Decomposition Energies ($\Delta E_{D,min,mutual}$) of the Interfaces among NYC, NYB, and Cathode Materials[a]

C_{SSE}	$C_{electrode}$	x_m	phase equilibria at x_m	$\Delta E_{D,min,mutual}$ (meV/atom)	$\Delta E_{D,min,total}$ (meV/atom)
NYC	$NaCoO_2$	0.45	NaCl, Y_2O_3, $NaClO_4$, Co_3O_4	−122	−125
	$NaCrO_2$	0.45	$YCrO_3$, NaCl, Cr_2O_3	−105	−109
	Na_2FePO_4F	0.43	Fe_2PO_4F, NaCl, YPO_4, YF_3	−70	−74
	$Na_3V_2(PO_4)_3$	0.60	NaCl, YPO_4, VCl_3	−50	−55
	$Na_3V_2(PO_4)_2F_3$	0.62	NaCl, YPO_4, VCl_3, YF_3	−41	−46
NYB	$NaCoO_2$	0.53	NaBr, Y_2O_3, Br, Co_3O_4	−127	−127
	$NaCrO_2$	0.45	$YCrO_3$, NaBr, Cr_2O_3	−110	−110
	Na_2FePO_4F	0.43	Fe_2PO_4F, NaBr, YPO_4, YF_3	−75	−75
	$Na_3V_2(PO_4)_3$	0.33	NaBr, YPO_4, VPO_4	−49	−49
	$Na_3V_2(PO_4)_2F_3$	0.36	NaBr, VPO_4, YF_3	−35	−35

[a]C_{SSE} and $C_{electrode}$ are the compositions of SSE and electrode materials, respectively, and x_m is the molar fraction of the SSE at the minimum reaction energy.

studies on the performance of yttrium halides as solid electrolytes for Na-ion batteries. As opposed to the previous study, the unique geometry endows the systems with high performance. We confirmed the fast Na^+ diffusion (0.77 and 0.44 mS/cm) in NYC and NYB due to the unique geometry and inherent vacancy carriers. In addition, the excellent electrochemical stability is well revealed by simulating the grand potential phase equilibrium, which shows that both NYC and NYB have wide electrochemical windows (0.51−3.75 and 0.57−3.36 V, respectively). Moreover, NYC and NYB exhibit good interfacial stability with Na metal anode and high-potential polyanion (fluoro)phosphate cathode materials, which can lead to efficient all-solid-state batteries with high voltage and high energy density. We hope that these attractive properties will stimulate more experimental effort in exploring halide-based SSEs, going beyond sulfide and oxide electrolytes.

■ ASSOCIATED CONTENT

Supporting Information

The Supporting Information is available free of charge at https://pubs.acs.org/doi/10.1021/acs.jpclett.0c00010.

Additional data and figures, including site ordering, phase stability, Na-ion migration and conductivity, electrochemical stability, chemical interface stability with cathode materials, phase equilibria, and minimum decomposition energies (PDF)

■ AUTHOR INFORMATION

Corresponding Author

Qiang Sun − *Department of Materials Science and Engineering and Center for Applied Physics and Technology, Peking University, Beijing 100871, China;* orcid.org/0000-0003-3872-7267; Email: sunqiang@pku.edu.cn

Authors

Yu Qie − *Department of Materials Science and Engineering, Peking University, Beijing 100871, China;* orcid.org/0000-0003-1404-8534

Shuo Wang − *Department of Materials Science and Engineering, Peking University, Beijing 100871, China;* orcid.org/0000-0002-7907-9676

Sijie Fu − *Department of Materials Science and Engineering, Peking University, Beijing 100871, China*

Huanhuan Xie − *Department of Materials Science and Engineering, Peking University, Beijing 100871, China;* orcid.org/0000-0002-3292-9039

Puru Jena − *Department of Physics, Virginia Commonwealth University, Richmond, Virginia 23284, United States;* orcid.org/0000-0002-2316-859X

Complete contact information is available at: https://pubs.acs.org/10.1021/acs.jpclett.0c00010

Author Contributions

Y.Q. and S.W. contributed equally to this work.

Notes

The authors declare no competing financial interest.

■ ACKNOWLEDGMENTS

This work was partially supported by grants from the National Natural Science Foundation of China (21973001) and from the National Key Research and Development Program of China (2016YFB0100200). S.W. appreciates the financial support from the China Scholarship Coucil. P.J. acknowledges partial support by the U.S. Department of Energy, Office of Basic Energy Sciences, Division of Materials Sciences and Engineering, under Award DE-FG02-96ER45579. The calculations were supported by the High-performance Computing Platform of Peking University.

■ REFERENCES

(1) Tarascon, J. M.; Armand, M. Issues and challenges facing rechargeable lithium batteries. *Nature* **2001**, *414* (6861), 359−367.

(2) Ellis, B. L.; Nazar, L. F. Sodium and sodium-ion energy storage batteries. *Curr. Opin. Solid State Mater. Sci.* **2012**, *16* (4), 168−177.

(3) Kim, S. W.; Seo, D. H.; Ma, X.; Ceder, G.; Kang, K. Electrode Materials for Rechargeable Sodium-Ion Batteries: Potential Alternatives to Current Lithium-Ion Batteries. *Adv. Energy Mater.* **2012**, *2* (7), 710−721.

(4) Larcher, D.; Tarascon, J. M. Towards greener and more sustainable batteries for electrical energy storage. *Nat. Chem.* **2015**, *7* (1), 19−29.

(5) Ponrouch, A.; Marchante, E.; Courty, M.; Tarascon, J.-M.; Palacín, M. R. In search of an optimized electrolyte for Na-ion batteries. *Energy Environ. Sci.* **2012**, *5* (9), 8572−8583.

(6) Zhao, L.; Zhao, J.; Hu, Y.-S.; Li, H.; Zhou, Z.; Armand, M.; Chen, L. Disodium Terephthalate (Na2C8H4O4) as High Performance Anode Material for Low-Cost Room-Temperature Sodium-Ion Battery. *Adv. Energy Mater.* **2012**, *2* (8), 962−965.

(7) Ding, C.; Nohira, T.; Kuroda, K.; Hagiwara, R.; Fukunaga, A.; Sakai, S.; Nitta, K.; Inazawa, S. NaFSA−C1C3pyrFSA ionic liquids for sodium secondary battery operating over a wide temperature range. *J. Power Sources* **2013**, *238*, 296−300.

(8) Hu, Y.-S. Batteries: Getting solid. *Nat. Energy* **2016**, *1*, 16042.

(9) Janek, J.; Zeier, W. G. A solid future for battery development. *Nat. Energy* **2016**, *1*, 16141.
(10) Hueso, K. B.; Armand, M.; Rojo, T. High temperature sodium batteries: status, challenges and future trends. *Energy Environ. Sci.* **2013**, *6* (3), 734.
(11) Wei, T.; Gong, Y.; Zhao, X.; Huang, K. An All-Ceramic Solid-State Rechargeable Na+-Battery Operated at Intermediate Temperatures. *Adv. Funct. Mater.* **2014**, *24* (34), 5380−5384.
(12) Tanibata, N.; Hayashi, A.; Tatsumisago, M. Improvement of Rate Performance for All-Solid-State Na15Sn4/Amorphous TiS3 Cells Using 94Na3PS4·6Na4SiS4 Glass-Ceramic Electrolytes. *J. Electrochem. Soc.* **2015**, *162* (6), A793−A795.
(13) Yue, J.; Han, F.; Fan, X.; Zhu, X.; Ma, Z.; Yang, J.; Wang, C. High-Performance All-Inorganic Solid-State Sodium-Sulfur Battery. *ACS Nano* **2017**, *11* (5), 4885−4891.
(14) Yue, J.; Zhu, X.; Han, F.; Fan, X.; Wang, L.; Yang, J.; Wang, C. Long Cycle Life All-Solid-State Sodium Ion Battery. *ACS Appl. Mater. Interfaces* **2018**, *10* (46), 39645−39650.
(15) Banerjee, A.; Park, K. H.; Heo, J. W.; Nam, Y. J.; Moon, C. K.; Oh, S. M.; Hong, S. T.; Jung, Y. S. Na3 SbS4: A Solution Processable Sodium Superionic Conductor for All-Solid-State Sodium-Ion Batteries. *Angew. Chem., Int. Ed.* **2016**, *55* (33), 9634−8.
(16) Chu, I. H.; Kompella, C. S.; Nguyen, H.; Zhu, Z.; Hy, S.; Deng, Z.; Meng, Y. S.; Ong, S. P. Room-Temperature All-solid-state Rechargeable Sodium-ion Batteries with a Cl-doped Na3PS4 Superionic Conductor. *Sci. Rep.* **2016**, *6*, 33733.
(17) Noguchi, Y.; Kobayashi, E.; Plashnitsa, L. S.; Okada, S.; Yamaki, J.-i. Fabrication and performances of all solid-state symmetric sodium battery based on NASICON-related compounds. *Electrochim. Acta* **2013**, *101*, 59−65.
(18) Hooper, A. A study of the electrical properties of single-crystal and polycrystalline β-alumina using complex plane analysis. *J. Phys. D: Appl. Phys.* **1977**, *10* (11), 1487−1496.
(19) Anantharamulu, N.; Koteswara Rao, K.; Rambabu, G.; Vijaya Kumar, B.; Radha, V.; Vithal, M. A wide-ranging review on Nasicon type materials. *J. Mater. Sci.* **2011**, *46* (9), 2821−2837.
(20) Goodenough, J. B.; Hong, H. Y. P.; Kafalas, J. A. Fast Na+-ion transport in skeleton structures. *Mater. Res. Bull.* **1976**, *11* (2), 203−220.
(21) Lalère, F.; Leriche, J. B.; Courty, M.; Boulineau, S.; Viallet, V.; Masquelier, C.; Seznec, V. An all-solid state NASICON sodium battery operating at 200 °C. *J. Power Sources* **2014**, *247*, 975−980.
(22) Hayashi, A.; Noi, K.; Sakuda, A.; Tatsumisago, M. Superionic glass-ceramic electrolytes for room-temperature rechargeable sodium batteries. *Nat. Commun.* **2012**, *3*, 856.
(23) Richards, W. D.; Tsujimura, T.; Miara, L. J.; Wang, Y.; Kim, J. C.; Ong, S. P.; Uechi, I.; Suzuki, N.; Ceder, G. Design and synthesis of the superionic conductor Na10SnP2S12. *Nat. Commun.* **2016**, *7*, 11009.
(24) Tanibata, N.; Noi, K.; Hayashi, A.; Tatsumisago, M. Preparation and characterization of highly sodium ion conducting Na3PS4−Na4SiS4 solid electrolytes. *RSC Adv.* **2014**, *4* (33), 17120−17123.
(25) Asano, T.; Sakai, A.; Ouchi, S.; Sakaida, M.; Miyazaki, A.; Hasegawa, S. Solid Halide Electrolytes with High Lithium-Ion Conductivity for Application in 4 V Class Bulk-Type All-Solid-State Batteries. *Adv. Mater.* **2018**, *30* (44), 1803075.
(26) Wang, S.; Bai, Q.; Nolan, A. M.; Liu, Y.; Gong, S.; Sun, Q.; Mo, Y. Lithium Chlorides and Bromides as Promising Solid-State Chemistries for Fast Ion Conductors with Good Electrochemical Stability. *Angew. Chem., Int. Ed.* **2019**, *58* (24), 8039−8043.
(27) Li, X.; Liang, J.; Luo, J.; Norouzi Banis, M.; Wang, C.; Li, W.; Deng, S.; Yu, C.; Zhao, F.; Hu, Y.; Sham, T.-K.; Zhang, L.; Zhao, S.; Lu, S.; Huang, H.; Li, R.; Adair, K. R.; Sun, X. Air-stable Li3InCl6 electrolyte with high voltage compatibility for all-solid-state batteries. *Energy Environ. Sci.* **2019**, *12*, 2665.
(28) Li, X.; Liang, J.; Chen, N.; Luo, J.; Adair, K. R.; Wang, C.; Banis, M. N.; Sham, T.-K.; Zhang, L.; Zhao, S.; Lu, S.; Huang, H.; Li, R.; Sun, X. H2O-Mediated Synthesis of Superionic Halide Solid Electrolyte. *Angew. Chem., Int. Ed.* **2019**, *58*, 16427.
(29) Kresse, G.; Furthmüller, J. Efficient iterative schemes for ab initio total-energy calculations using a plane-wave basis set. *Phys. Rev. B: Condens. Matter Mater. Phys.* **1996**, *54* (16), 11169−11186.
(30) Blöchl, P. E. Projector augmented-wave method. *Phys. Rev. B: Condens. Matter Mater. Phys.* **1994**, *50* (24), 17953−17979.
(31) Perdew, J. P.; Burke, K.; Ernzerhof, M. Generalized Gradient Approximation Made Simple. *Phys. Rev. Lett.* **1996**, *77* (18), 3865−3868.
(32) Heyd, J.; Scuseria, G. E. Efficient hybrid density functional calculations in solids: Assessment of the Heyd−Scuseria−Ernzerhof screened Coulomb hybrid functional. *J. Chem. Phys.* **2004**, *121* (3), 1187−1192.
(33) Heyd, J.; Scuseria, G. E.; Ernzerhof, M. Erratum: "Hybrid functionals based on a screened Coulomb potential" [J. Chem. Phys. 118, 8207 (2003)]. *J. Chem. Phys.* **2006**, *124* (21), 219906.
(34) Jain, A.; Ong, S. P.; Hautier, G.; Chen, W.; Richards, W. D.; Dacek, S.; Cholia, S.; Gunter, D.; Skinner, D.; Ceder, G.; Persson, K. A. Commentary: The Materials Project: A materials genome approach to accelerating materials innovation. *APL Mater.* **2013**, *1* (1), 011002.
(35) Mo, Y.; Ong, S. P.; Ceder, G. First Principles Study of the Li10GeP2S12 Lithium Super Ionic Conductor Material. *Chem. Mater.* **2012**, *24* (1), 15−17.
(36) Ong, S. P.; Richards, W. D.; Jain, A.; Hautier, G.; Kocher, M.; Cholia, S.; Gunter, D.; Chevrier, V. L.; Persson, K. A.; Ceder, G. Python Materials Genomics (pymatgen): A robust, open-source python library for materials analysis. *Comput. Mater. Sci.* **2013**, *68*, 314−319.
(37) He, X.; Zhu, Y.; Mo, Y. Origin of fast ion diffusion in superionic conductors. *Nat. Commun.* **2017**, *8*, 15893.
(38) He, X.; Zhu, Y.; Epstein, A.; Mo, Y. Statistical variances of diffusional properties from ab initio molecular dynamics simulations. *npj Comput. Mater.* **2018**, *4* (1), 18.
(39) Ong, S. P.; Wang, L.; Kang, B.; Ceder, G. Li−Fe−P−O2 Phase Diagram from First Principles Calculations. *Chem. Mater.* **2008**, *20* (5), 1798−1807.
(40) Zhu, Y.; He, X.; Mo, Y. Origin of Outstanding Stability in the Lithium Solid Electrolyte Materials: Insights from Thermodynamic Analyses Based on First-Principles Calculations. *ACS Appl. Mater. Interfaces* **2015**, *7* (42), 23685−93.
(41) Han, F.; Zhu, Y.; He, X.; Mo, Y.; Wang, C. Electrochemical Stability of Li10GeP2S12 and Li7La3Zr2O12 Solid Electrolytes. *Adv. Energy Mater.* **2016**, *6* (8), 1501590.
(42) Zhu, Y.; He, X.; Mo, Y. First principles study on electrochemical and chemical stability of solid electrolyte−electrode interfaces in all-solid-state Li-ion batteries. *J. Mater. Chem. A* **2016**, *4* (9), 3253−3266.
(43) Asano, T.; Sakai, A.; Ouchi, S.; Sakaida, M.; Miyazaki, A.; Hasegawa, S. Solid Halide Electrolytes with High Lithium-Ion Conductivity for Application in 4 V Class Bulk-Type All-Solid-State Batteries. *Adv. Mater.* **2018**, *30* (44), 1803075.
(44) Liang, J.; Li, X.; Wang, S.; Adair, K. R.; Li, W.; Zhao, Y.; Wang, C.; Hu, Y.; Zhang, L.; Zhao, S.; Lu, S.; Huang, H.; Li, R.; Mo, Y.; Sun, X. Site-Occupation-Tuned Superionic LixScCl3+x Halide Solid Electrolytes for All-Solid-State Batteries. *J. Am. Chem. Soc.* **2020**, DOI: 10.1021/jacs.0c00134.
(45) Aono, H.; Sugimoto, E.; Sadaoka, Y.; Imanaka, N.; Adachi, G.-y. Ionic conductivity and sinterability of lithium titanium phosphate system. *Solid State Ionics* **1990**, *40*−*41*, 38−42.
(46) Mo, Y.; Ong, S. P.; Ceder, G. First Principles Study of the Li10GeP2S12 Lithium Super Ionic Conductor Material. *Chem. Mater.* **2012**, *24* (1), 15−17.
(47) Murugan, R.; Thangadurai, V.; Weppner, W. Fast Lithium Ion Conduction in Garnet-Type Li7La3Zr2O12. *Angew. Chem., Int. Ed.* **2007**, *46* (41), 7778−7781.
(48) Thangadurai, V.; Narayanan, S.; Pinzaru, D. Garnet-type solid-state fast Li ion conductors for Li batteries: critical review. *Chem. Soc. Rev.* **2014**, *43* (13), 4714−4727.

https://dx.doi.org/10.1021/acs.jpclett.0c00010
J. Phys. Chem. Lett. 2020, 11, 3376−3383

(49) Kim, J.-K.; Lim, Y. J.; Kim, H.; Cho, G.-B.; Kim, Y. A hybrid solid electrolyte for flexible solid-state sodium batteries. *Energy Environ. Sci.* **2015**, *8* (12), 3589−3596.
(50) Stenzel, F.; Meyer, G. Ternäre Halogenide vom Typ A3MX6. II. Das System Ag3−xNaxYCl6: Synthese, Strukturen, Ionenleitfähigkeit. *Z. Anorg. Allg. Chem.* **1993**, *619* (4), 652−660.
(51) Huang, H.; Wu, H. H.; Wang, X.; Huang, B.; Zhang, T. Y. Enhancing sodium ionic conductivity in tetragonal-Na3PS4 by halogen doping: a first principles investigation. *Phys. Chem. Chem. Phys.* **2018**, *20* (31), 20525−20533.
(52) Tang, H.; Deng, Z.; Lin, Z.; Wang, Z.; Chu, I.-H.; Chen, C.; Zhu, Z.; Zheng, C.; Ong, S. P. Probing Solid−Solid Interfacial Reactions in All-Solid-State Sodium-Ion Batteries with First-Principles Calculations. *Chem. Mater.* **2018**, *30* (1), 163−173.
(53) Komaba, S.; Nakayama, T.; Ogata, A.; Shimizu, T.; Takei, C.; Takada, S.; Hokura, A.; Nakai, I. Electrochemically Reversible Sodium Intercalation of Layered NaNi0.5Mn0.5O2 and NaCrO2. *ECS Trans.* **2008**, *16* (42), 43−55.
(54) Ellis, B. L.; Makahnouk, W. R.; Makimura, Y.; Toghill, K.; Nazar, L. F. A multifunctional 3.5 V iron-based phosphate cathode for rechargeable batteries. *Nat. Mater.* **2007**, *6* (10), 749−53.
(55) Ellis, B. L.; Makahnouk, W. R. M.; Rowan-Weetaluktuk, W. N.; Ryan, D. H.; Nazar, L. F. Crystal Structure and Electrochemical Properties of A2MPO4F Fluorophosphates (A = Na, Li; M = Fe, Mn, Co, Ni)†. *Chem. Mater.* **2010**, *22* (3), 1059−1070.
(56) Kim, S. W.; Seo, D. H.; Kim, H.; Park, K. Y.; Kang, K. A comparative study on Na2MnPO4F and Li2MnPO4F for rechargeable battery cathodes. *Phys. Chem. Chem. Phys.* **2012**, *14* (10), 3299−303.
(57) Jian, Z.; Han, W.; Lu, X.; Yang, H.; Hu, Y.-S.; Zhou, J.; Zhou, Z.; Li, J.; Chen, W.; Chen, D.; Chen, L. Superior Electrochemical Performance and Storage Mechanism of Na3V2(PO4)3Cathode for Room-Temperature Sodium-Ion Batteries. *Adv. Energy Mater.* **2013**, *3* (2), 156−160.
(58) Song, W.; Cao, X.; Wu, Z.; Chen, J.; Zhu, Y.; Hou, H.; Lan, Q.; Ji, X. Investigation of the Sodium Ion Pathway and Cathode Behavior in Na3V2(PO4)2F3 Combined via a First Principles Calculation. *Langmuir* **2014**, *30* (41), 12438−12446.
(59) Han, F.; Westover, A. S.; Yue, J.; Fan, X.; Wang, F.; Chi, M.; Leonard, D. N.; Dudney, N. J.; Wang, H.; Wang, C. High electronic conductivity as the origin of lithium dendrite formation within solid electrolytes. *Nature Energy* **2019**, *4* (3), 187−196.
(60) Ramachandran, R.; Saranya, M.; Santhosh, C.; Velmurugan, V.; Raghupathy, B. P. C.; Jeong, S. K.; Grace, A. N. Co9S8 nanoflakes on graphene (Co9S8/G) nanocomposites for high performance supercapacitors. *RSC Adv.* **2014**, *4* (40), 21151−21162.
(61) Song, W.; Ji, X.; Wu, Z.; Zhu, Y.; Yao, Y.; Huangfu, K.; Chen, Q.; Banks, C. E. Na2FePO4F cathode utilized in hybrid-ion batteries: a mechanistic exploration of ion migration and diffusion capability. *J. Mater. Chem. A* **2014**, *2* (8), 2571.

https://dx.doi.org/10.1021/acs.jpclett.0c00010
J. Phys. Chem. Lett. 2020, 11, 3376−3383